Green Chemistry

PAPER

View Article Online
View Journal | View Issue

Cite this: *Green Chem.*, 2024, **26**, 3418

Green fabrication of fabric by ethanol/water solvent-mediated self-assembly of homogeneous lignin for oil–water separation†

Xinlu Liu,[a,b] Shuzhen Ni, *[a,b] Xiaoqian Chen, *[a,b] Zongquan Li,[a,b] Yingjuan Fu,[a,b] Menghua Qin[c] and Fengshan Zhang[d]

Received 29th October 2023,
Accepted 29th January 2024

DOI: 10.1039/d3gc04160c

rsc.li/greenchem

The utilization of lignin in material fabrication has garnered significant attention despite its complex structure that greatly limits its applications. This study reports a green method for grading and modifying lignin to prepare stable hydrophobic coatings *via* the solvent/anti-solvent (ethanol/water) self-assembly method. First, the formic acid lignin particle (FLP) is prepared and the underlying mechanism is primarily ascribed to the hydrogen bonding, π–π interactions among aromatic groups within and between molecules, and hydrophobic interactions. The lignin nanoparticles were utilized to chelate with metal ions (iron) in order to obtain the stable hydrophobic coatings using the special nanostructures of FLP. This hydrophobic coating could be applied to different substrates (blocks, straw, and fabric). The cotton fabric exhibited an initial water contact angle (WCA) that increased from 73.4° to 129.6°, and excellent chemical and physical hydrophobic performance. Moreover, this coating has strong self-cleaning ability and could be used for oil–water separation. In this newly proposed fabrication, ethanol can be recovered in the preparation of lignin nanoparticles, which makes the green and facile preparation of a stable hydrophobic coating possible. Additionally, this work is important in upgrading formic acid lignin by controlling the polarity into value-added hydrophobic materials *via* green classification.

1. Introduction

The interest in surfaces with special wettability has surged in recent years because of their relevance to fundamental research and potential applications, such as oil/water separation,[1] self-cleaning,[2,3] antipollution,[4] anticorrosion[5] batteries, anti-icing coatings, sensors, and antibioadhesion. A well-known method of obtaining hydrophobic properties involves the creation of artificial surfaces that mimic natural materials (*e.g.* lotus leaves)[6] by reducing the surface energy (*e.g.* with materials containing fluorine and silicon).[7] This can be achieved by processes such as the sol–gel technique,[8] electrospinning,[9] chemical etching,[10,11] layer by layer self-assembly,[12] and chemical vapor deposition.[13,14] These techniques are guided by conventional theory (Cassie–Baxter model) that describes the range of surface wettability from hydrophilicity to hydrophobicity.[14]

To achieve this, numerous works have been carried out. Fu *et al.* prepared a hydrophobic film with a water contact angle value of 140°, which is coated with hexadecyltrimethoxysilane (HDTMS) *via* chemical vapor deposition.[15] Zhao *et al.* introduced transparent and durable superhydrophobic coatings with the water contact angle up to 166.6° using the chemical vapor deposition of polydimethylsiloxane.[16] Nevertheless, the practical utilization of these materials is constrained by intricate processing steps, elevated costs, substrate limitations, as well as issues concerning the mechanical durability and chemical stability. Besides, the involved fluorine-containing or silicone-containing reagents are harmful to the environment and human health and do not comply with the sustainability concept. Therefore, it is necessary to develop green materials with excellent durability using low energy consumption methods.

Metal phenolic networks (MPNs) are regarded as popular candidates used in surface modification or functionalization of substrates.[17,18] The system efficiently creates micro-/nano-coatings on templates, utilizing the dynamic coordination of metal ions and phenolic ligands, to improve the substrate's hydrophobic properties.[19] Liu *et al.*

[a]*Key Laboratory of Pulp and Paper Science & Technology of Ministry of Education, Faculty of Light Industry, China. E-mail: nishuzhen@qlu.edu.cn, chenxiaoqian1208@163.com*
[b]*State Key Laboratory of Biobased Material and Green Papermaking, Faculty of Light Industry, Qilu University of Technology (Shandong Academy of Sciences), Jinan 250353, China*
[c]*College of Chemistry and Chemical Engineering, Qilu Normal University, Jinan 250200, China*
[d]*Shandong Huatai Paper Co., Ltd & Shandong Yellow Triangle Biotechnology Industry Research Institute Co. Ltd, China*

† Electronic supplementary information (ESI) available. See DOI: https://doi.org/10.1039/d3gc04160c

obtained a super-hydrophobic coating using lauryl gallate (LG) and Fe^{2+} with WCA values of 136.6°. Long *et al.* constructed core@shell MOF materials to obtain powders with superhydrophobicity *via* MPN.[20]

As a polyphenolic compound, lignin has attracted significant attention in recent years as an abundant, renewable and environmental-friendly phenolic biopolymer in the pursuit of sustainable resource utilization and development of biomass-based functional materials.[21] It is abundantly produced as a by-product of the bio-refinery and papermaking sectors, which might pollute the environment and cause a tremendous waste of resources when not adequately managed. Another noteworthy issue is the heterogeneous structure and complex functional groups (including aryl ring structures, aliphatic, aromatic hydroxyl groups, reactive groups and methoxy groups) within the macromolecules, which would greatly affect its physicochemical properties and diverse applications. In particular, the hydroxyl groups and aromatic structures are the most critical functional groups that determine the performance of the polymers.[22,23] Until now, lignin was mainly dumped or burned to produce heat. Furthermore, only 2% was utilized as commercial chemicals, such as absorbents,[24] dispersants,[25,26] surfactants,[27] and antibacterial materials.[28] Thus, it is crucial to develop new avenues to highly and efficiently utilize lignin through technological advancement.

However, lignin is a three-dimensional heterogeneous biopolymer.[29] Many techniques have been used to synthesize a wide range of lignin derivatives, including esterification,[30] silylation,[31] and oxidation/reduction.[32] Graded separation represents an efficient approach to mitigate lignin heterogeneity, offering a promising avenue to enhance the value-added utilization of lignin. Presently, lignin graded separation processes fall into three distinct categories: acid precipitation,[33] stepwise solvent separation[34] and membrane separation.[35] In the context of acid precipitation, lignin colloidal surfaces are negatively charged and necessitate neutralization through the addition of acid, which unfortunately offers limited separation efficiency. Moreover, the substantial generation of acidic water presents an environmental concern. On the other hand, membrane separation technology relies on molecular weight, but the typically low solubility of lignin frequently leads to membrane contamination. This, in turn, reduces the treatment capacity and shortens the membrane lifespan. In contrast, solvent-based fractionation hangs on variations in the solubility and polarity of lignin, accounting for different molecular weights and functional groups in organic solvents such as tetrahydrofuran, dimethyl sulfoxide, and methanol. This approach is deemed efficient and controllable, with the added benefit of recyclability.[36] Utilizing this method, lignin readily self-assembles into spherical nanoparticles through solvent/anti-solvent self-assembly, exemplified by systems like THF/water and acetic acid/hexane.[37–40] Lignin nanoparticles exhibit excellent physicochemical properties with high surface area-to-volume ratios and a large amount of surface functional groups. Zhang *et al.* obtained UV-blocking sunscreen through the preparation of light-colored lignin.[41] Gonçalves *et al.* prepared lignin-silica hybrid nanocomposite films to improve the hydrophobic behavior of the hybrid film.[42] Currently, most solvents have high or low toxicity, and can seriously pollute the environment. Such solvents include ethyl acetate,[43] methanol, methylene chloride, *N*,*N*-dimethylformamide (DMF), tetrahydrofuran, and acetone. Therefore, researchers synthesized lignin nanoparticles through green solvents like ethylene glycol and γ-valerolactone (GVL).[44] Ethanol is a green solvent due to its remarkable selectivity for lignin and its environmental friendliness.

In this work, lignin graded separation was carried out using the ethanol/water system. The resultant lignin is used to chelate with metals to form a metal-phenolic network structure. In comparison with our previous report, the lignin/metal particles deposited on fabrics form an excellent hydrophobic coating with a water contact angle value of 149.9°. However, there still exist certain drawbacks, such as the instability of the hydrophobic coatings and excessive usage of water during the preparation of lignin nanoparticles *via* dialysis.[45] Herein, we adopted relatively homogeneous lignin nanoparticles by means of a green solvent/anti-solvent (ethanol/water) method, which helps in the preparation of a stable hydrophobic coating and reduced consumption of water. In summary, an effective hydrophobic coating was generated through the chelation of graded formic acid lignin particles with iron ions, resulting in micro/nanostructures deposited onto a substrate. The chosen lignin exhibited heightened reactivity due to its substantial phenolic hydroxyl group content.[46] Initially, the ethanol/water self-assembly of lignin was assessed for various physicochemical properties, including the particle size, potential, molecular weight, hydroxyl group content and surface morphology. The lignin that underwent iron chelation was subject to FT-IR, UV and ^{31}P NMR analysis. Subsequently, the hydrophobic characteristics of the coating layer on the fabric were evaluated using SEM, AFM and WCA measurements. The resulting fabric demonstrated the ability to perform oil–water separation and proved effective in treating oil spills, while maintaining exceptional stability, practicality, and self-cleaning properties. Additionally, the raw material (lignin) used is a by-product of the pulp and paper-making process, which can improve the utilization value of lignin. Compared with other studies of preparing lignin-based hydrophobic materials, this method does not use any fluorine-containing and silane-based hydrophobic reagents, which is in line with the green chemistry process.[47] Furthermore, this preparation method enriches the spectrum of lignin utilization in the realm of hydrophobic coatings. It offers a cost-effective, straightforward and environmentally-friendly approach in alignment with the sustainable principle to prepare FLP nanoparticles and functional hydrophobic cotton fabric.

2. Materials and methods

2.1 Materials

Cotton fabric (100% cotton) of 235.38 g m^{-2} was obtained from a waste lab coat. All cotton fabrics were washed with

ethanol and deionized water before use. Ferric chloride, ethanol, hexane, toluene, petroleum ether, trichloromethane, dichloromethane, tetrachloromethane and tetrahydrofuran were purchased from Shanghai Maclin Biochemical Co., Ltd. 2-Chloro-4,4,5,5-tetramethyl-1,3,2-dioxaphospholan (TMDP) was provided by Sigma Aldrich (Shanghai) Trading Co., Ltd. Formic acid lignin (FAL) was obtained from the black liquor of Shandong Shengle Co., Ltd. Deionized water was obtained in the laboratory.

2.2 Preparation of formic acid lignin particles (FLP)

Formic acid lignin particles were meticulously prepared through a series of steps. Initially, the black liquor was transformed into formic acid lignin particles (FLP) *via* aqueous precipitation, with a water-to-black liquor volume ratio of 30 : 1 (v/v). Subsequently, FLP underwent further processing through a gradient ethanol/water solvent system to generate diverse lignin variants. Specifically, the lignin was solubilized in anhydrous ethanol at room temperature, employing continuous magnetic stirring at 500 rpm, thus yielding a 1 mg ml^{-1} lignin solution. This solution was then gradually diluted with deionized water at a rate of 2 ml min^{-1}, resulting in the formation of aqueous FLP dispersions. Furthermore, a centrifugation at 7000 rpm for 6 minutes enabled the separation of dissolved and insoluble fractions of lignin. The soluble lignin, subsequently isolated and freeze-dried, was denoted as FLP-100, FLP-60, FLP-50, FLP-40, and FLP-20. Specifically, the FLP represents formic acid lignin particles and the numbers indicate the volume percentage of ethanol in the mixed solution after the addition of the anti-solvent.

2.3 Preparation of FLP/Fe@cotton fabric

FLP, in ethanol or ethanol/water solution, was mixed with iron at a ratio of 1 : 1 (w/w) to obtain the FLP/Fe hydrophobic coating solution. The pre-treated fabric was immersed in the FLP/Fe solution at 45 °C for 24 hours. After the surface deposition, the fabric was rinsed with deionized water and dried at 45 °C for 6 hours. The preparation process of the FLP/Fe@cotton fabric is shown in Scheme 1.

2.4 Characterizations

Several characterizations were performed to gain insight into the materials. The size and zeta potential of FLPs in the solvent were determined using a DLS instrument (Nano-ZS90, Malvern, UK), while the ethanol content decreased from 100% to 20% at 25 °C. In this experiment, the refractive indexes of ethanol and acetone were used as 1.630 and 1.356, respectively. The FTIR spectra of the FLPs and FLP/Fe particles were recorded using a Bruker (Germany) microscopic infrared spectrometer in the range of 4000 cm^{-1} to 500 cm^{-1}. Gel permeation chromatography (GPC) (Waters, USA) of acetylated formic acid lignin particles in THF (2 mg mL^{-1}) was conducted with a 10 μm Mixed-E 7.5 mm ID column coupled with UV detector at 254 nm. Reflectance spectra of FLP were measured using a UV-2600 spectrometer (Shimadzu, Japan). The ^{31}P NMR of FLP was conducted with a spectrometer (Bruker AV III 400 M) to record the chemical groups. In brief, the formic acid lignin particles (20 mg) were dissolved in a deuterated pyridine/deuterated chloroform mixture. The internal standard solution and phosphorylated reagent were then added, and measured after 15 minutes. Additionally, the FLPs, FLP/Fe, FLP@cotton fabric, and FLP/Fe@cotton fabric were examined using SEM (scanning electron microscope, HITACH, Japan), with samples being coated with gold powder. AFM (atomic force microscope, Bruker, Germany) was employed to assess the surface morphology of the fabrics.

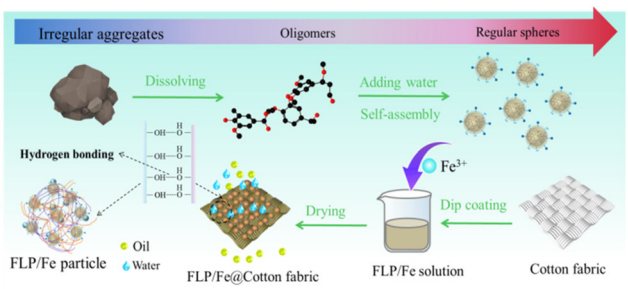

Scheme 1 The preparation process of the FLP/Fe@cotton fabrics.

2.5 Water contact angle (WCA)

The wettability of the cotton fabrics was evaluated through water contact angle (WCA) testing. Five drops of distilled water were used for each sample, and the WCAs were recorded using an OCA50 (DATAPHYSICS, OCA50, Germany) apparatus.

2.6 Self-cleaning performance

The self-cleaning performance was assessed using mud. The cotton fabric was positioned on an inclined table, and a solution (slurry, 5 : 4 ratio) was injected onto the surface. A parallel test was conducted with methylene blue powder, where the powder was dispersed on the tilted cotton fabric, and a small drop of water was injected onto the fabric. The results were recorded, and the behavior of the mud and methylene blue on the fabric was observed.

2.7 Oil–water separation

This test was performed for both heavy and floating oil. To facilitate observation, the oil and water were dyed with oil red O and methylene blue, respectively. Dichloroethane was chosen as the circulating experimental oil. The separation flux (Q, L m^{-2} h^{-1}) was obtained using eqn (1):

$$Q = V/At \quad (1)$$

Here, V (L), A (m^2) and t (h) stand for the volume of the oil, filtration area and time, respectively. The separation efficiency (η, %) was obtained according to eqn (2):

$$\eta = M_1/M_0 \times 100\% \quad (2)$$

In this equation, M_1 (g) and M_0 (g) represent the mass of the filtrate oil and the mass of the initial oil, respectively.

2.8 Stability and suitability

The FLP-50/Fe@cotton fabric was analyzed to assess the stability and suitability. The friction resistance test involved a 100 g weight attached to the FLP-50/Fe@cotton fabric, which was then rubbed for 1000 cycles. Contact angles were measured both before and after the abrasion tests. Furthermore, we exposed the FLP-50/Fe@cotton fabric to extreme conditions: 105 °C (GZX-9146MBE, China), −20 °C (Haier Zhijia Co., Ltd, China), and 375 nm UV light for 12 hours to assess its resistance to high temperatures, low temperatures, and UV radiation. To evaluate chemical stability, the FLP-50/Fe@cotton fabric was tested separately with HCl (pH = 2), NaCl (saturated solution, pH = 7), NaOH (pH = 12), ethanol and acetone for 12 hours. The broad applicability of the coating with the FLP-50/Fe solution on some substrates, including wood blocks, straw, and fabrics (65% polyester–35% cotton and 80% polyester–20% cotton), was conducted.

3. Results and discussion

3.1 Analysis of formic acid lignin particles (FLP)

The structural composition and molecular weight of lignin play a pivotal role in determining its physicochemical properties and diverse applications. Lignin exhibits the intriguing ability to self-assemble when subjected to a combination of ethanol and water, acting as a solvent and anti-solvent, respectively. The creation of FLP solutions is achieved by precisely adjusting the ratio of water added. As depicted in Fig. 1a, with the addition of the anti-solvent (water), the FLP-100, FLP-60, FLP-50, FLP-40, and FLP-20 solutions undergo two changes: from turbid to clear, and then to turbid again. This is due to the fact that the solubility of FLP increases and then decreases, and FLP has a maximum solubility in 50% ethanol, which can be seen from the inset bottle figures in Fig. 1a. This intriguing behavior can be ascribed to the enhanced content of hydrogen bonds resulting from the mixture of water and organic solvents, which, in turn, augments lignin's solubility.[48] These findings imply potential disparities in the chemical structure among the various FLPs. Therefore, a comprehensive examination was undertaken to meticulously scrutinize the trends in molecular weight and chemical functionality of the FLPs. The ensuing results are presented for detailed analysis.

In Fig. 1a, the UV absorption of the FLP solution reveals the presence of two distinct absorption peaks in each FLP. These peaks are approximately centered at 216 nm and 279 nm, and are ascribed to the unsaturated structure and the phenoxy ring structure, respectively.[49] It is worth noting the blue shift of the absorption peak at 216 nm with the introduction of a highly polar solvent–water. This shift is a result of the heightened solvation effect on unbound electrons and the absorption peak of the n → π* transition, which typically shifts to shorter wavelengths as the solvent's polarity increases.[50,51]

FTIR spectra provide insight into the chemical structure of the samples, and are a valuable tool for lignin characterization. The FTIR spectra of the FLP components, as depicted in Fig. 1b, clearly resemble typical lignin IR absorption patterns. The absorption band at 3414 cm^{-1} is broad, and attributed to the hydroxyl groups of aliphatic and phenolic compounds. The peaks of 2933 cm^{-1} and 2843 cm^{-1} correspond to the stretching vibrations (C–H) from methyl groups. The signals at 1599 cm^{-1} are associated with aromatic ring vibrations, while the signal at 1461 cm^{-1} is indicative of methoxyl bending (C–H) and stretching (C–C) within the aromatic skeleton. The characteristic adsorptions at 1120 cm^{-1} and 1030 cm^{-1} are caused by syringyl (S) and guaiacyl (G), respectively. With the addition of an anti-solvent (from FLP-100 to FLP-20), the characteristic adsorptions at 3414 cm^{-1}, 1120 cm^{-1} and 1030 cm^{-1} changed. These changes indicate fluctuations in the relative content of the functional groups of the FLP moieties with the different solvent system.[52] The quantitative result of the hydroxyl groups in FLP *via* ^{31}P NMR is presented in Fig. 1c, revealing distinct signals associated with specific hydroxyl groups. In the spectrum, the signal ranging from 150.0 to 145.4 ppm corresponds to aliphatic OH, while the signals within the ranges of 144.4–140.2 ppm, 140.2–137.4 ppm and 137.4–136.0 ppm refer to the syringyl OH (S), guaiacyl OH (G) and *p*-hydroxyphenyl OH (H), respectively. Additionally, the signal at 135.5–132.8 ppm is indicative of carboxylic acid OH (COOH).[53] The details of these functional group contents can be found in Table S1.† Notably, FLP-20 exhibits the highest total phenolic OH content (3.93 mmol g^{-1}). As depicted in Fig. 1d, the zeta potentials of FLP-100 to FLP-20 gradually decrease. While FLP-40 contains lower levels of phenolic OH or carboxyl groups compared to FLP-100, FLP-60 and FLP-50, it exhibits a higher negative zeta potential (−57.6 mV). This phenomenon can be explained by the smaller particle size of FLP-40 and FLP-20, which results in a larger specific surface area and a relatively greater number of functional groups on the nanoparticle surface.

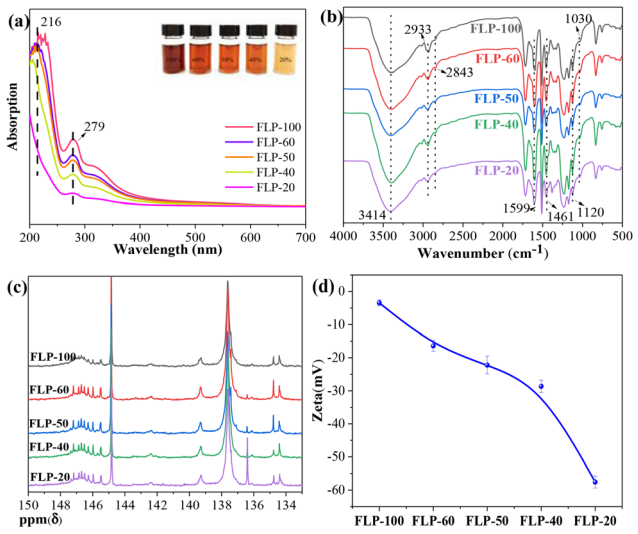

Fig. 1 (a) UV–vis spectra, (b) FTIR, (c) ^{31}P NMR and (d) zeta potential of FLP solution or particles.

3.2 Morphology of FLP

As illustrated in Fig. 2b, the solutions of FLPs in pure ethanol displayed a broad size distribution of hydraulic radii, ranging from several dozen nanometers to microscopic dimensions. This variation is a consequence of lignin's inherent polydisperse nature. However, when the ethanol volume ratio drops to 60% or lower, the soluble FLP molecules coalesce into monomodally distributed nanoparticles, with DLS of 712.4 nm, 617.1 nm, 341.6 nm, and 343 nm for FLP-60, FLP-50, FLP-40, and FLP-20, respectively (Fig. 2b). This aggregation is driven by the increased attraction between the lignin molecules with higher moisture content in the solvent mixture.[54]

SEM images of FLP provided in Fig. 2 offer a more visually intuitive examination of their morphology. FLP-10 appears as irregular fragments of varying sizes (Fig. 2a1 and a2), while FLP-60 (Fig. 2c1 and c2) exhibits a spherical structure with a wrinkled surface. Remarkably, the average size of FLP-50 (Fig. 2d1 and d2), FLP-40 (Fig. 2e1 and e2) and FLP-20 (Fig. 2f1 and f2) progressively assumes smooth, spherical shapes with diminishing diameters, as evident in the accompanying histogram (Fig. 2c3–f3). This observed transformation aligns with the results obtained *via* DLS (Fig. 2b). The aggregation of lignin molecules into nanospheres can be attributed to the intermolecular interactions between the solvent and anti-solvent (ethanol and water) during the production of lignin nanoparticles. This nanosphere formation is suggested to result from van der Waals interactions and π–π interactions among the hydrophobic groups, including aliphatic carbon chains and aromatic rings, found in lignin molecules.[55] Additionally, the GPC analysis of the molecular weight distribution in the three lignin fractions demonstrates a gradual reduction in molecular weight throughout the fractionation process (Table S2†).

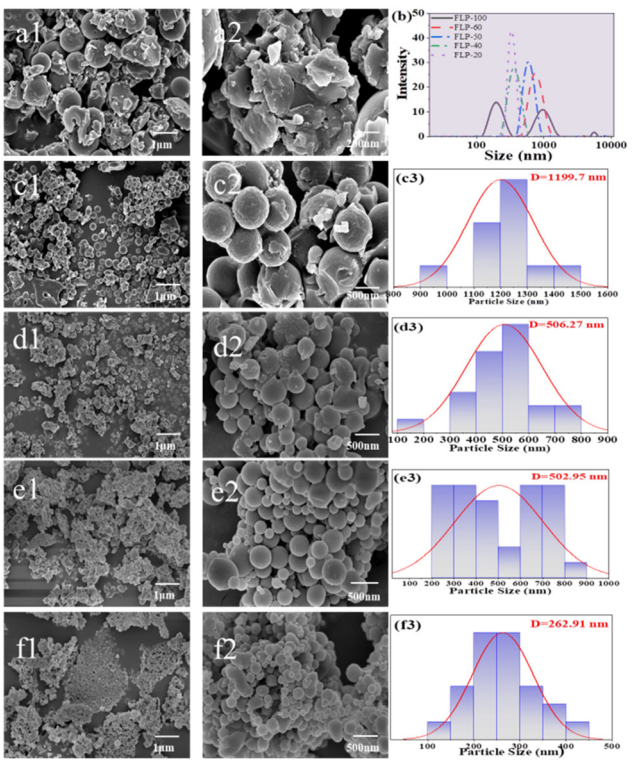

Fig. 2 SEM images of FLP-100 (a1 and a2), FLP-60 (c1 and c2), FLP-50 (d1 and d2), FLP-40 (e1 and e2), FLP-20 (f1 and f2), particle size histogram of FLP-100 to FLP-20 (c3, d3, e3 and f3) calculated from images of c2, d2, e2, f2 and the DLS size of FLPs (b). The 'D' term and bell curve in c3, d3, e3, f3 represent the average particle size and the corresponding distribution of average particle size after calculation, respectively.

3.3 Hydrophobicity of FLP/Fe@cotton fabrics

The hydrophobicity of the lotus leaf's surface is a well-known phenomenon attributed to the presence of numerous waxy protruding substances. When a lotus leaf is submerged in water, it exhibits a silvery luminescent surface, a result of air pockets forming on its surface. In this study, it has been observed that lignin's chelation with metal ions in MPN formation leads to the development of stable micro/nanostructures on fabric surfaces through hydrogen bonding.[45] To investigate this, the FLP-50@cotton fabric was selected for a silver mirror test (Fig. S2†), in which a similar silvery shimmering effect was observed. This can be attributed to the creation of air pockets, reducing the contact area between water molecules and the fabric.

To further assess the impact of self-assembly and metal-phenolic network (MPN) on hydrophobicity, we conducted contact angle measurements on pristine cotton fabric, FLP@cotton fabrics, and FLP/Fe@cotton fabrics (Fig. 3). The pristine cotton fabric exhibits extremely hydrophilic characteristics, boasting an initial contact angle of 73.4°, with water droplets completely absorbed within a mere second. The FLP@cotton fabric displays an improved initial contact angle exceeding 110°, but falters in hydrophobic stability (Fig. 3a), as water droplets are absorbed within 14 seconds. This is attributed to the self-assembly of lignin, which enhances the fabric's roughness, but with less uniformity.

In stark contrast, the FLP/Fe@cotton fabric showcases an excellent water contact angle (WCA) value of 120° and maintains its hydrophobicity for a prolonged duration, remaining hydrophobic even after 30 minutes (Fig. 3b). Surprisingly, the FLP-50/Fe@cotton fabric attained a water contact angle value of 149°. Notably, the FLP-50/Fe@cotton fabric and FLP-60/Fe@cotton fabric achieved remarkable WCAs of 120°, retaining their outstanding hydrophobicity for up to 50 minutes (as

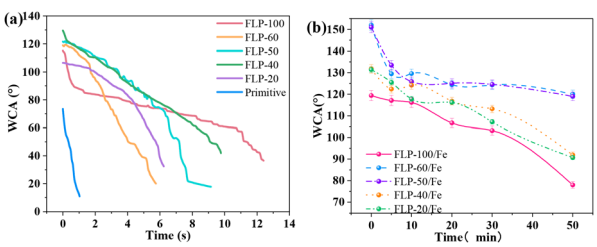

Fig. 3 (a) The WCA values of cotton fabrics deposited by (a) FLP and (b) FLP/Fe.

observed in the accompanying Video S1†). This exceptional performance can be attributed to the presence of uniform, near-spherical, three-dimensional surface structures on the FLP-50/Fe@cotton fabric and FLP-60/Fe@cotton fabric. Consequently, the FLP-50/Fe@cotton fabric was selected for further investigations into coating stability and performance.

3.4 Chemical structure analysis of FLP/Fe

The self-assembly of lignin plays a pivotal role in metal ion chelation, resulting in changes in the molecular weight, particle size, and the number of functional groups. To analyze these effects, we examined the UV absorption spectra of FLP and FLP/Fe. As depicted in Fig. S3,† the absorption peaks of FLP-100 to FLP-50 at 279 nm exhibit a gradual decrease, with FLP-40 and FLP-20 showing no absorption peaks at this wavelength. Conversely, the absorption peaks of FLP/Fe at 216 nm show a blue shift, indicating a reaction between the iron ions and lignin that shifts the maximum absorption peaks to shorter wavelengths. Furthermore, the FTIR spectra of FLP are presented in Fig. S4,† with peak intensities of FLP/Fe at 1030–1120 cm^{-1} weaker than FLP, indicating a chelation of lignin's hydroxyl groups with iron. The vibrations at 2935 cm^{-1} and 2847 cm^{-1}, as well as the peak at 1707 cm^{-1}, disappear in FLP-60/Fe, FLP-50/Fe, FLP-40/Fe, and FLP-20/Fe, compared to FLP-100/Fe. This is ascribed to the self-loading of the graded lignin-ferric iron on the fabric surface *via* the MPN reaction. These studies collectively support the notion that coordination occurs between lignin and metal ions.

The wetting behavior of a material is intrinsically linked to its hierarchical micro/nanostructures and surface chemical composition. To confirm surface chemical changes between the pristine cotton fabric and FLP-50/Fe@ cotton fabric, X-ray photoelectron spectroscopy (XPS) data for C, O, and Fe binding energies were collected and are shown in Fig. 4a. The C 1s spectrum of the fabrics reveals four distinct peaks at about 287.3 eV, 285.6 eV, 284.2 eV, and 283.7 eV, corresponding to the O–C–C, C–OH, C–C(C–H), and C=C moieties, respectively (Fig. 4b). Notably, the relative C–C content increases to 22% from 12% due to the lignin deposition (Table S3†). In the O 1s spectrum (Fig. 4c and d), the peaks at 532.1 eV, 532.7 eV, and 534.6 eV represent the C–O–C, O–H, and C–O bonds, respectively. The C–O, O–H and Fe–C–O group contents increase to 42%, 3% and 2% from 33%, 2% and 0%, respectively, while the C–O–C group content decreases from 65% to 53% (Table S4†). The new peak at 531.2 eV is the Fe–O–C bond in the FLP-50/Fe@cotton fabric, which indicates the deposition of Fe on the cotton surface. The relatively higher content of O–H linkages in the FLP-50/Fe@cotton fabric also confirms the adhesion of FLP-50/Fe *via* hydrogen bonding (Table S4†). To analyze the valence of iron in pristine fabric and the FLP-50/Fe@cotton fabric, the high-resolution Fe 2p spectra are shown in Fig. 4e and f. The photoelectron peaks at 725.7 eV and 711.3 eV (ref. 56 and 57) correspond to the characteristic doublet Fe 2p1/2 and Fe 2p3/2, respectively, confirming the presence and deposition of iron on the surface of

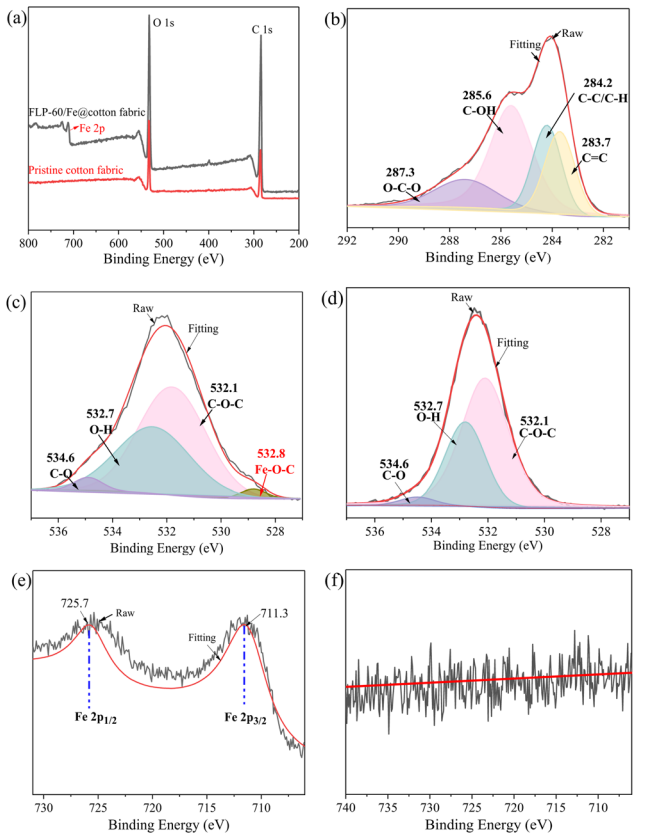

Fig. 4 Wide XPS spectra of (a) pristine fabric, high resolution C 1s (d) and Fe 2p (f) of the pristine fabric; and high-resolution O 1s (b), C 1s (c) and Fe 2p (e) spectra of the FLP-50/Fe@cotton fabric.

the FLP-50/Fe@cotton fabric. In comparison, there was no significant Fe 2p feature on the pristine fabric (Fig. 4f).

3.5 Morphology of cotton fabrics

Fig. 5 displays the SEM images of the FLP@cotton fabrics. The pristine fabric surface is notably smooth with no discernible raised structures (Fig. 5f1 and f2). The fabric deposited with FLP exhibits a certain roughness, albeit with weak and irregular attachments (Fig. 5a1–e1). As a result, the FLP@cotton fabrics exhibit a slight increase in the initial water contact angle, but lack hydrophobic stability. This is due to the lignin particles' inability to form a uniform, specific structure attached to the cotton fabric.

In contrast, the surfaces of the FLP/Fe@cotton fabrics exhibit unique three-dimensional surface structures (Fig. 5a2–e3), significantly enhancing the hydrophobicity of the cotton fabrics. Notably, the near-spherical structures loaded onto the FLP-50/Fe@cotton fabric (Fig. 5c2 and c3), FLP-40/Fe@cotton fabric (Fig. 5d2 and d3), and FLP-20/Fe@cotton fabric (Fig. 5e2 and e3) contribute to their hydrophobic stability. Among these, the FLP-50/Fe@cotton fabric demonstrates superior hydrophobic stability. This is primarily due to the uniform nano size of the FLP-50 particles, which form near-spherical structure clusters that uniformly and compactly adhere to the

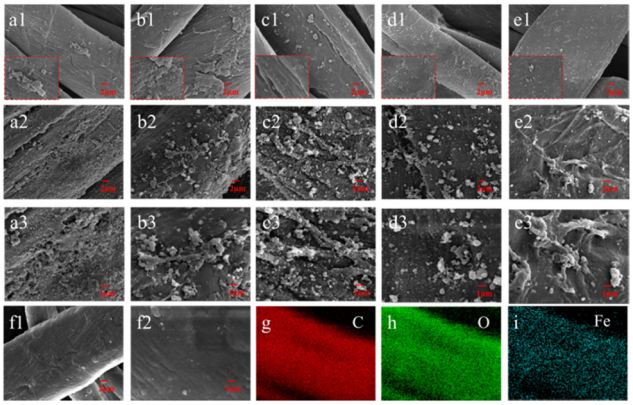

Fig. 5 SEM images of the FLP@cotton fabric (a1–e1), cotton fabrics deposited by FLP-100/Fe (a2 and a3), FLP-60/Fe (b2 and b3), FLP-50/Fe (c2 and c3), FLP-40/Fe (d2 and d3), FLP-20/Fe (e2 and e3) with two magnifications and pristine fabric (f1 and f2); the distribution of C (g), O (h) and Fe (i) element on the FLP-50/Fe@cotton fabric.

fabric's surface. The key factor behind the hydrophobic stability lies in the homogeneous near-spherical structure. The EDS element results of the FLP-50/Fe@cotton fabric (Fig. 5i) confirms that Fe attaches to the FLP-50@cotton fabric surface, leading to an increased Fe content compared with the pristine fabric (Fig. S6†).

The AFM characterization reveals an increase and subsequent decrease in fabric roughness (Fig. 6a–f). Remarkably, the FLP-50/Fe@cotton fabric exhibits a dramatic increase from 3.57 nm to 47.1 nm (a more than thirteen-fold increase, see Fig. 6a and d). This is attributed to the granular FLP that uniformly adheres to the fabric and forms micro–nano hillock protrusions. This property allows water droplets to rest on the FLP/Fe@cotton fabric for an extended period, facilitated by the ordered FLP/Fe structures on the surface that minimize the contact area, thereby reducing the surface tension and preventing water droplet adhesion. Reducing the surface energy is another vital factor in the creation of hydrophobic materials. The surface energy values (SE) for pristine and FLP/Fe-deposited cotton fabrics are assessed and displayed in Fig. 6g. The SE of pristine fabric is notably high at 879 mJ m^{-2}, making it susceptible to wetting by general droplets. After modification, the SE values for the fabrics (FLP-50/Fe@cotton fabric and FLP-40/Fe@cotton fabric) have an obvious decrease, compared with the surface tension of water (72.8 mN m^{-1}), indicating excellent repellent characteristics toward water molecules. The loading amount of FLP/Fe particles loaded on the cotton fabric follows a pattern of increase and decrease (Fig. 6h), aligning with the solubility of lignin in ethanol/water.

3.6 Mechanism

The coordination between formic acid lignin (FL) and iron plays a crucial role in the construction of micro/nanostructures when deposited onto substrates (Fig. 7). In prior research, we reported the development of hydrophobic coatings through

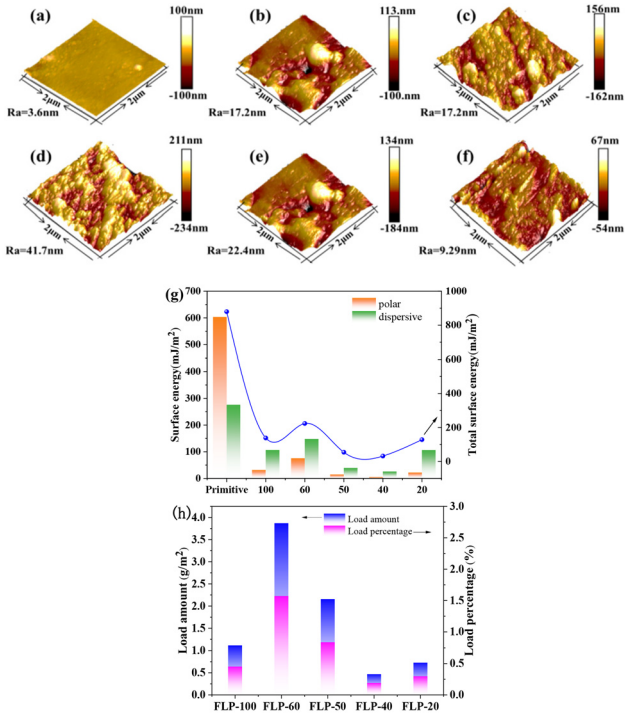

Fig. 6 AFM images of pristine (a), FLP-100/Fe@cotton fabric (b), FLP-60/Fe@cotton fabric (c), FLP-50/Fe@cotton fabric (d), FLP-40/Fe@cotton fabric (e), FLP-20/Fe@cotton fabric (f); (g) the surface energy of pristine and FLP/Fe-deposited cotton fabrics; (h) the FLP/Fe load amount and percentage on fabrics.

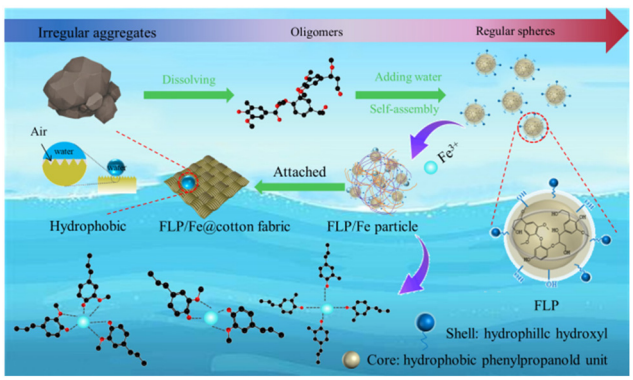

Fig. 7 The self-assembly mechanism of formic acid lignin particles and formation of micro/nano structures *via* FLP/Fe coordination.

the reaction of formic acid lignin obtained *via* rotary evaporation with iron. However, these coatings exhibited poor stability.[45] In this experiment, we employed a solvent/antisolvent method (utilizing ethanol/water) to create uniform formic acid lignin particles (FLPs) through self-assembly. Previous studies have indicated that the self-assembly of lignin compounds is driven by hydrogen bonding, π–π interactions among aromatic groups within and between molecules, and hydrophobic interactions.[58,59] As the water content in the system increased,

the polar segment of formic acid lignin compounds exhibited an affinity for water, leading to an escalation in the polar group content (carboxyl, hydroxyl). Conversely, the water molecules around the non-polar hydrophobic skeleton were excluded and repelled, therefore stabilizing the contact of non-polar regions. This phenomenon induced the π–π stacking, resulting in the assembly of spherical FLP structures and a reduction in size.

The structure of FLP significantly influences its reactivity with ions. The adjacent hydroxyl groups in formic acid lignin particles possess chelating sites that can react with ions to form stable metal phenolic networks (MPNs). We demonstrated that FLP forms chelates with ferric ions, a conclusion supported by infrared (IR), ultraviolet (UV), and X-ray photoelectron spectroscopy (XPS) analyses. Formic acid lignin (in various forms: FLP-100, FLP-60, FLP-50, FLP-40, and FLP-20) and iron first interact to create differently shaped FLP/Fe particles, which subsequently deposit onto fabric in clusters driven by intermolecular forces. This deposition of FLP/Fe particles imparts high hydrophobicity to the fabrics, enhancing the surface roughness and lowering the surface energy (Fig. 8). Notably, the presence of uniform and suitably sized FLP/Fe particles contributes to the superior hydrophobic stability. This might be determined by multiple factors, including the M_w, Ar-OH and –COOH groups of FLP.

During the deposition of FLP/Fe on cotton fabric, the assembly of FLP and the chelation of FLP/Fe occurs simultaneously. With the addition of water, FLP would spontaneous self-assemble into spherical particles, while the particle size gradually decreased. However, the chelation between FLP and Fe relies on the phenolic hydroxyl groups and carboxyl groups of FLP, which would affect the assembly of FLP and the autonomous loading. FLP-20 and FLP-40 have higher zeta potentials, enabling them to more easily chelate with iron. For FLP-20, due to its relatively larger specific surface area (smaller particle size) and higher hydroxyl group content, the phenolic hydroxyl group tend to chelate with iron, while reducing the deposition as assembled spherical particles on the fabric. This may be seen from Fig. 5e2 and e3, which show that less spherical particles are found on the FLP-20/Fe@cotton fabric.

3.7 Stability and durability

The mechanical durability of the FLP-50/Fe@cotton fabric in the face of physical damage holds significant importance for practical applications (Fig. 9). After 1000 rubbings, the WCA value of the FLP-50/Fe@cotton fabric remains impressively high at 130°, retaining its strong hydrophobicity. The corresponding SEM images illustrates that a substantial number of FLP-50/Fe particles remained and were firmly attached to the fabric. This robust adhesion indicates that FLP-50/Fe particles establish strong bonds with the fabric, offering substantial friction resistance. Furthermore, the FLP-50/Fe@cotton fabric exhibited high oil–water separation efficiency (98.0%) and flux (625 L m^{-1} h^{-2}) after 1000 frictions (shown in Video S3†). Even under the stress of high temperature (105 °C), low temperature (−20 °C), and UV irradiation (375 nm) for 12 hours, the initial WCA values for the FLP-50/Fe@cotton fabric retain high levels, with water droplets maintaining their position for over 30 minutes. The corresponding WCAs were 129.6°, 135.6°, and 137°, respectively. This phenomenon underscores the excellent stability of the FLP-50/Fe@cotton fabric. The FLP-50/Fe@cotton fabric also shows great durability after multiple washing cycles (Fig. S7†). After 20 laundry cycles, the water contact angle value reaches 128.9°. Even after 100 cycles, the fabric still remains hydrophobic (the water contact angle value is 102.4°), which indicates that the FLP-50/Fe@cotton fabric possesses good stability.

Hydrophobic coatings that exhibit chemical resistance are in high demand. To assess the chemical stability of the FLP-50/Fe@cotton fabric, we subjected it to HCl (pH = 2), NaCl (pH = 7), NaOH (pH = 12), ethanol, and acetone treat-

		FLP-100	FLP-60	FLP-50	FLP-40	FLP20
FLP	Mw	2867	2705	2741	2551	2500
	Ar-OH$_{(mmol/g)}$	3.21	3.80	3.79	3.58	3.93
	-COOH$_{(mmol/g)}$	0.28	0.38	0.38	0.31	0.34
FLP/Fe@cotton fabric	SE(mJ/m^2)	138.16	223.26	54.29	22.4	9.29
	Ra(nm)	17.9	27.0	47.1	22.4	9.29
	AFM					
	WCA	78°	119°	120°	91.9°	90.7°

Fig. 8 The main experimental results for supporting mechanisms (the WCA is tested when the water droplet stays for 50 min).

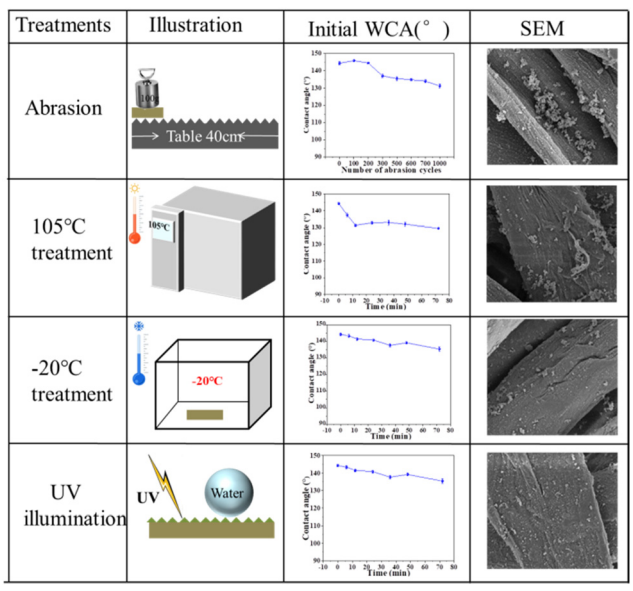

Fig. 9 Initial water contact angles and SEM of the FLP-50/Fe@cotton fabric by different treatments.

ments for 12 hours, evaluating the hydrophobicity through the initial water contact angles. The results reveal that the FLP-50/Fe@cotton fabric demonstrates outstanding stability upon treatment with acids, alkaline salts, and organic solvents, maintaining contact angles above 130° (Table 1, left). Remarkably, in acidic and alkaline salt environments, water droplets can remain on the surface for up to 30 minutes, demonstrating the suitability of the FLP-50/Fe coating as a protective layer against chemical attacks. Excitingly, FLP-50/Fe can be effectively deposited on a variety of substrates (Table 1, right) to enhance their hydrophobicity (Fig. S8†), including wood, straw, and composite fabrics (comprising 65% polyester–35% cotton and 80% polyester–20% cotton).

3.8 Self-cleaning performance

This hydrophobic coating allows water droplets to efficiently roll off, carrying dirt and debris with them, resulting in a self-cleaning surface. Muddy substances quickly slide off the FLP-50/Fe@cotton fabric surface, leaving dirt on the original fabric (as observed in the accompanying Video S2† and Fig. 10a1 and a2). Furthermore, the self-cleaning capability of the FLP-50/Fe@cotton fabric was tested by methylene blue. We found that water can take away methylene blue powders from the FLP-50/Fe@cotton fabric surface (Fig. 10b1 and b2). This underscores the fabric's commendable self-cleaning performance.

3.9 Oil–water separation performance

Oil–water separation technology plays a crucial role in addressing marine oil spill pollution. The remarkable hydrophobic and lyophilic properties of the FLP-50/Fe@cotton fabric make it highly suitable for efficient oil–water separation. We conducted gravity-driven oil–water separation tests using simulated oils, including trichloromethane, dichloromethane, and tetrachloromethane. Compared with other lignin-based hydrophobic materials in previous work, it can be seen that our modified fabrics with the excellent separation properties are green, without using any toxic reagents or high-cost silanes, as shown in Table S5.† The oil–water separation tests utilized hexane, toluene, and petroleum ether as the simulated oils. The outcomes unequivocally demonstrate oil–water separation efficiencies exceeding 98.3%, with dichloromethane showcasing exceptional separation efficiency and flux of 99.6% and 669 L m^{-1} h^{-2}, respectively (as seen in Fig. 11a). Remarkably,

Table 1 Water contact angles of the FLP-50/Fe@cotton fabric by different treatments (left) and deposition on different substrates (right)

Treatments	Initial WCA (°)	Composition	Initial WCA (°)	
			Primitive	Modified
HCl (pH = 2)	136.3	Wood	77.8	136.2
NaCl (pH = 7)	141.0	Straw	83.1	139.8
NaOH (pH = 12)	139.0	65% polyester–35% cotton	20.1	138.2
Ethanol	130.0	80% polyester–20% cotton	0	139.5
Acetone	135.3	100% cotton	73	149

Fig. 10 Images of the anti-fouling performance of the (a1) pristine cotton fabric and (a2) FLP-50/Fe@cotton fabric. Self-cleaning performance of the (b1) pristine cotton fabric and (b2) FLP-50/Fe@cotton fabric.

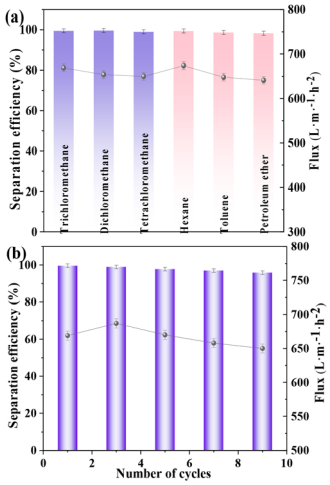

Fig. 11 (a) The separation performance of the FLPL-50/Fe@cotton fabric; (b) the separation efficiency of the FLPL-50/Fe@cotton fabric for dichloromethane with different numbers of cycles.

the FLP-50/Fe@cotton fabric exhibits outstanding durability. As illustrated in Fig. 11b, after 10 separation cycles, the separation efficiency and capacity for dichloroethane remained high at 95.9% and 650 L m^{-1} h^{-2}, respectively. The decrease in the separation efficiency or capacity was not significant, underscoring the fabric's excellent reusability.

4. Conclusions

A durable hydrophobic coating was grafted onto cotton fabric *via* the solvent/anti-solvent self-assembly strategy. Formic acid lignin particles (FLP) were first prepared by self-assembly in ethanol/water. Then, the FLP was chelated with iron ions and deposited onto the fabric to form a homogeneous special

rough structure. The FLP-50/Fe@cotton fabric exhibits extremely stable hydrophobicity with a water contact angle value of 142°. Particularly, the FLP-50/Fe@cotton fabric has excellent self-cleaning and oil–water separation performance, showcasing exceptional separation efficiency (99.6%) and flux (669 L m^{-1} h^{-2}) towards dichloromethane, and has superior recycling ability. More significantly, the FLP-50/Fe hydrophobic coating can be applied to a wide range of substrates. These significant advances pave the way of the practical application of lignin-based hydrophobic coatings in self-cleaning and bulk oil/water mixture separation.

Author contributions

Xinlu Liu: implementation of experimental protocols, analysis of data and writing of paper. Shuzhen Ni: ideas; formulation or evolution of overarching research goals and aims. Xiaoqian Chen: domestic and international research, and feasibility study analyses. Zongquan Li: writing – reviewing & editing. Yingjuan Fu: supervision, validation. Menghua Qin: methodology, supervision.

Conflicts of interest

The authors declare that they have no known competing financial interests or personal relationships that could have appeared to influence the work reported in this paper.

Acknowledgements

This research study is supported by the National Natural Science Foundation of China (22208175) and (32271821), QUTPY Project (2023PY032) and QUTPX Project (2023PX020), and the Jinan Independently Cultivate Innovative Team (202228076).

References

1 X. Liu, S. Ni, W. Yang, X. Chen, Y. Zhang, Z. Li, H. Xie, Y. Li, Y. Fu and M. Qin, *Appl. Surf. Sci.*, 2023, **637**, 157655.
2 Z. Zhou, Q. Zhu, Y. Liu, Y. Zhang, Z. Jia and G. Wu, *Nano-Micro Lett.*, 2023, **15**, 137.
3 B. Wang, Z. Yin, W. Cheng, Y. Zhang and Y. Hu, *Composites, Part A*, 2023, **166**, 107392.
4 Y. Shen, Z. Wu, J. Tao, Z. Jia, H. Chen, S. Liu, J. Jiang and Z. Wang, *ACS Appl. Mater. Interfaces*, 2020, **12**, 25484–25493.
5 B.-H. Li, S.-L. Wang, S. Pal, P. B. So, G.-Y. Chen, W.-J. Huang, Y.-L. Hsu, S.-Y. Kuo, J.-M. Yeh and C.-H. Lin, *Microporous Mesoporous Mater.*, 2021, **325**, 111319.
6 P. Nguyen-Tri, H. N. Tran, C. O. Plamondon, L. Tuduri, D.-V. N. Vo, S. Nanda, A. Mishra, H.-P. Chao and A. K. Bajpai, *Prog. Org. Coat.*, 2019, **132**, 235–256.
7 G. J. Puts, P. Crouse and B. M. Ameduri, *Chem. Rev.*, 2019, **119**, 1763–1805.
8 R. R. Hashjin, Z. Ranjbar, H. Yari and G. Momen, *Surf. Interfaces*, 2022, **33**, 102282.
9 A. Raman, J. S. Jayan, B. D. S. Deeraj, A. Saritha and K. Joseph, *Surf. Interfaces*, 2021, **24**, 101140.
10 A. Kumar and B. Gogoi, *Tribol. Int.*, 2018, **122**, 114–118.
11 Y. Ye, Z. Kang, F. Wang, Y. Long, T. Guo, D. Chen, J. Kong and L. Xu, *Appl. Surf. Sci.*, 2023, **610**, 155362.
12 Q. Xie, G. Yin, Q. Duan, Y. Zhong, J. Xie, K. Fu and P. Wang, *Polym. Compos.*, 2023, **44**, 6071–6082.
13 Y. Cao, Y. Lu, N. Liu, Y. Li, P. Wang, C. Dai and Y. Wei, *Surf. Interfaces*, 2022, **32**, 102100.
14 R. Pan, M. Cai, W. Liu, X. Luo, C. Chen, H. Zhang and M. Zhong, *J. Mater. Chem. A*, 2019, **7**, 18050–18062.
15 Q. Fu, K. Tu, C. Goldhahn, T. Keplinger, M. Adobes-Vidal, M. Sorieul and I. Burgert, *ACS Nano*, 2020, **14**, 13775–13783.
16 X. Zhao, B. Yu and J. Zhang, *J. Colloid Interface Sci.*, 2017, **501**, 222–230.
17 K. Tu, B. Puértolas, M. Adobes-Vidal, Y. Wang, J. Sun, J. Traber, I. Burgert, J. Pérez-Ramírez and T. Keplinger, *Adv. Sci.*, 2020, **7**, 1902897.
18 Z. Yang, Z. Zhou, H. Guo, Z. Yao, X. Ma, X. Song, S.-P. Feng and C. Y. Tang, *Environ. Sci. Technol.*, 2018, **52**, 9341–9349.
19 J. Chen, S. Pan, J. Zhou, R. Seidel, S. Beyer, Z. Lin, J. J. Richardson and F. Caruso, *Chem. Mater.*, 2021, **33**, 2557–2566.
20 Y. Long, L. Xiao, Q. Cao, X. Shi and Y. Wang, *Chem. Commun.*, 2017, **53**, 10831–10834.
21 S. Iravani and R. S. Varma, *Green Chem.*, 2020, **22**, 612–636.
22 C. Chio, M. Sain and W. Qin, *Renewable Sustainable Energy Rev.*, 2019, **107**, 232–249.
23 W. Schutyser, T. Renders, S. V. den Bosch, S.-F. Koelewijn, G. T. Beckham and B. F. Sels, *Chem. Soc. Rev.*, 2018, **47**, 852–908.
24 T. Wang, M. Jiang, X. Yu, N. Niu and L. Chen, *Sep. Purif. Technol.*, 2022, **302**, 122116.
25 J. Yang, X. Wang and H. Liu, *ACS Sustainable Chem. Eng.*, 2023, **11**, 8199–8207.
26 X. Xiao, J. Jiang, Y. Wang, B. Wang, T.-Q. Yuan, Q. Shi, X. Liao, B. Shi and R.-C. Sun, *ACS Sustainable Chem. Eng.*, 2021, **9**, 9053–9061.
27 S. Bertella, M. B. Figueirêdo, G. De Angelis, M. Mourez, C. Bourmaud, E. Amstad and J. S. Luterbacher, *ChemSusChem*, 2022, **15**, e202200270.
28 K. Li, W. Zhong, P. Li, J. Ren, K. Jiang and W. Wu, *Int. J. Biol. Macromol.*, 2023, **252**, 126281.
29 B. Wang, Y.-C. Sun and R.-C. Sun, *Collagen Leather*, 2019, **1**, 5.
30 Y. Yan, L. Zhang, X. Zhao, S. Zhai, Q. Wang, C. Li and X. Zhang, *Int. J. Biol. Macromol.*, 2022, **203**, 49–57.
31 Y.-H. Jiang, Y.-Q. Zhang, C. Gao, Q.-D. An, Z.-Y. Xiao and S.-R. Zhai, *Sep. Purif. Technol.*, 2022, **282**, 120138.
32 Y. Qi, B. Liu, X. Qiu, X. Zeng, Z. Luo, W. Wu, Y. Liu, L. Chen, X. Zu, H. Dong, X. Lin and Y. Qin, *Adv. Mater.*, 2023, **35**, 2208284.

33 X. Cao, L. Shao, W. Huang, C. Wang, J. Mao, F. Xu and X. Zhang, *J. Anal. Appl. Pyrolysis*, 2021, **157**, 105200.
34 Y. Xu, L. Hu, H. Huang, D. Tong and C. Hu, *Carbohydr. Polym.*, 2012, **88**, 1342–1347.
35 D. Huang, R. Li, P. Xu, T. Li, R. Deng, S. Chen and Q. Zhang, *Chem. Eng. J.*, 2020, **402**, 126237.
36 A.-S. Jääskeläinen, T. Liitiä, A. Mikkelson and T. Tamminen, *Ind. Crops Prod.*, 2017, **103**, 51–58.
37 X. Wu, H. Lian, X. Li and J. Xiao, *Int. J. Biol. Macromol.*, 2023, **253**, 126664.
38 W. Jiang, S. Liu, C. Wu, Y. Liu, G. Yang and Y. Ni, *Green Chem.*, 2020, **22**, 8734–8744.
39 J. Huang, Q. Guo, R. Zhu, Y. Liu, F. Xu and X. Zhang, *Int. J. Biol. Macromol.*, 2021, **189**, 635–640.
40 X. Lu, Y. Zhang, J. Chen, D. Zhang, C. Dong, P. Zhiqiang and T. Xia, *Ind. Crops Prod.*, 2021, **172**, 113993.
41 J. Zhang, Z. Tian, X.-X. Ji and F. Zhang, *Int. J. Biol. Macromol.*, 2023, **231**, 123244.
42 G. C. Gonçalves, F. Gimeno, C. Dicharry, J. Allouche, F. C-E. Bouhtoury and J.-C. Dupin, *ACS Sustainable Chem. Eng.*, 2022, **10**, 12783–12795.
43 C. A. Mullen, G. D. Strahan and Y. Elkasabi, *J. Anal. Appl. Pyrolysis*, 2022, **164**, 105522.
44 F. Cheng, S. Liu, S. D. Karlen, H. Kim, F. Lu, J. Ralph, L. M. V. Ramos, G. W. Huber and J. A. Dumesic, *Green Chem.*, 2023, **25**, 336–347.
45 X. Liu, X. Chen, H. Bian, S. Ni, Z. Li, N. Liu, M. Qin and F. Zhang, *Ind. Crops Prod.*, 2023, **204**, 117393.
46 S. Ni, H. Bian, Y. Zhang, Y. Fu, W. Liu, M. Qin and H. Xiao, *Biomacromolecules*, 2022, **23**, 829–838.
47 P. Jessop, *Green Chem.*, 2020, **22**, 13–15.
48 H. Gao, M. Sun, Y. Duan, Y. Cai, H. Dai and T. Xu, *Int. J. Biol. Macromol.*, 2023, **246**, 125596.
49 Y. Wang, X. Xiao, S. Wang, K. Li, Y. Jiang, Y. Ma, T. Zhang and R. Ran, *J. Nat. Fibers*, 2021, **18**, 71–79.
50 A. Mookherji and S. P. Tandon, *J. Phys. Soc. Jpn.*, 1966, **21**, 1176–1178.
51 H. McConnell, *J. Chem. Phys.*, 2004, **20**, 700–704.
52 W. D. H. Schneider, A. J. P. Dillon and M. Camassola, *Biotechnol. Adv.*, 2021, **47**, 107685.
53 P. Figueiredo, M. H. Lahtinen, M. B. Agustin, D. M. de Carvalho, S.-P. Hirvonen, P. A. Penttilä and K. S. Mikkonen, *ChemSusChem*, 2021, **14**, 4718–4730.
54 J. Wang, W. Chen, D. Yang, Z. Fang, W. Liu, T. Xiang and X. Qiu, *Small*, 2022, **18**, 2200671.
55 L. Chen, S.-M. Luo, C.-M. Huo, Y.-F. Shi, J. Feng, J.-Y. Zhu, W. Xue and X. Qiu, *Green Chem.*, 2022, **24**, 285–294.
56 Q. Zhou, B. Yan, T. Xing and G. Chen, *Carbohydr. Polym.*, 2019, **203**, 1–9.
57 Q. Zhou, G. Chen and T. Xing, *Cellulose*, 2018, **25**, 1513–1525.
58 I. V. Pylypchuk, A. Riazanova, M. E. Lindström and O. Sevastyanova, *Green Chem.*, 2021, **23**, 3061–3072.
59 I. V. Pylypchuk, M. Karlsson, P. A. Lindén, M. E. Lindström, T. Elder, O. Sevastyanova and M. Lawoko, *Green Chem.*, 2023, **25**, 4415–4428.